Journal of Southeast University (English Edition) Vol. 27, No. 1, pp. 26 – 30 Mar. 2011 ISSN 1003—7985

Static characteristics of a novel flux-switching permanent magnet linear motor

Huang Lei Yu Haitao Hu Minqiang Zhou Shigui Liu Hexiang

(School of Electrical Engineering, Southeast University, Nanjing 210096, China)
(Engineering Research Center for Motion Control of Ministry of Education, Southeast University, Nanjing 210096, China)

Abstract: A novel flux-switching permanent magnet linear motor (FSPMLM) is proposed for linear direct driving machine tools. First, the two- and three-dimensional topological configuration of the proposed motor is presented; the basic operational principle of the FSPMLM is introduced; and the magnetic fields at the two typical conditions of no-load are analyzed. Secondly, the FSPMLM is analyzed by the two-dimensional finite element method (FEM) to investigate the static electromagnetic characteristics such as flux-linkage, back EMF (electromotive force) and inductance performances. The cogging forces of two kinds of FSPMLMs with different shaped cores are analyzed and compared, and the results show that the cogging force is significantly reduced by using the E-shaped cores. Additionally, based on the co-energy method, the thrust equation is derived and verified by the simulation results obtained by the FEM. Finally, an experimental prototype is used to test the characteristics under open circuit and load conditions. The simulation and experimental results indicate that the proposed motor has advantages of a sinusoidal back-EMF waveform, a small cogging effect and a high thrust density, and it is suitable for the application of linear direct driving machine tools.

Key words: flux-switching; permanent magnet linear motor; finite element method; static characteristics
doi: 10.3969/j.issn.1003 – 7985.2011.01.006

Linear machines have many advantages over rotary ones under long distance linear motion[1], such as linear direct driving machine tools. Among various linear motors, the linear induction machine (LIM) and the permanent magnet linear machine (PMLM) are the main research objects. The LIM can attract attention due to its simple structure and low costs. However, the low power factor, thrust density and efficiency are its shortcomings[2]. The PMLM can provide high power density, high thrust density and a high power factor. The traditional PMLMs, such as linear synchronous machines, are secondary-permanent magnet (PM) linear machines, which have the disadvantages of a complex PM structure and a high manufacturing cost[3]. Therefore, the primary-PM linear machine having magnets embedded in the primary iron core has been paid considerable attention for its advantages of having a simple secondary structure and low costs.

The FSPMLM is a kind of primary-PM linear machine. The concept of the rotational FSPM machine was first proposed by Rauch et al[4]. The planar linear FSPM machine was proposed and investigated by Wang et al[5]. Zhu and Wang et al.[6-7] proposed a tubular FSPMLM and a double-side FSPMLM. A method by using assistant teeth is employed to reduce the detent force [8], which is induced by slot effect and end effect. Based on the principle of the rotational FSPM machine, a novel linear FSPM brushless motor is presented for digital control processing of machine tools. The two-dimensional finite element method is used to analyze the proposed FSPMLM. The static characteristics of flux linkage, back-EMF, inductance, cogging force and thrust force of the FSPMLM are obtained. Several simulations are done by the finite element analysis (FEA). Finally, the simulation results are validated by using an experimental prototype. The results show that the proposed linear FSPMLM has better back-EMF waveform, smaller cogging force and thrust force ripple.

1 Topology and Operation Principle

The configuration of the proposed single-side long secondary FSPMLM is shown in Fig. 1. This kind of motor consists of a primary mover and a secondary stator. The long stator is a ferromagnetic steel plate including a plurality of teeth and slots. The mover is made up of three phase assemblies, i.e., phases A, B and C. There are two U-shaped and five E-shaped stacks in the mover. Two U-shaped stacks are installed in the ends, with E-shaped stacks in the middle of the mover. Each phase is comprised of one entire U-shaped stack and a portion of anther E-shaped stack or portions of two E-shaped stacks. Eight teeth in one phase assembly face the corresponding teeth or slots of the stator. Both the armature winding and permanent magnets are set on the short mover. The PMs are positioned between stacks, and coils are wound in the slots of each stack.

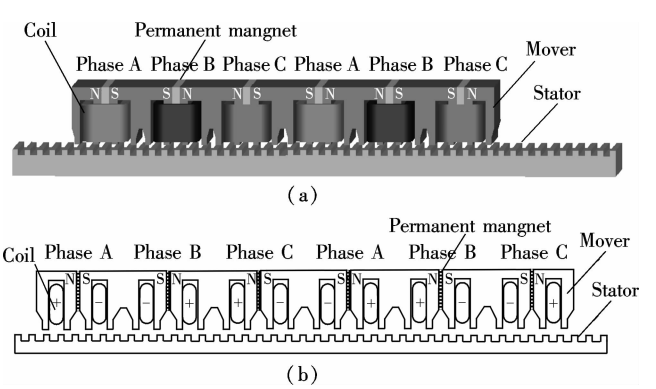

Fig. 1 The configuration of proposed FSPMLM. (a) The 3-D model of FSPMLM; (b) The 2-D model of FSPMLM

Received 2010-09-07.
Biographies: Huang Lei (1980—), male, graduate; Yu Haitao (corresponding author), male, doctor, professor, htyu@seu.edu.cn.
Citation: Huang Lei, Yu Haitao, Hu Minqiang, et al. Static characteristics of a novel flux-switching permanent magnet linear motor. [J]. Journal of Southeast University (English Edition), 2011, 27(1): 26 – 30. [doi: 10.3969/j.issn.1003 – 7985.2011.01.006]

In order to obtain the three phase sinusoidal back-EMF, the central axis of the first phase is offset from the second phase $(N \pm 2/3)\tau$, and the electrical angle is $(M180° \pm 120°)$, where M and N are integers, and τ, the distance between two teeth of the stator, is the pole pitch of the stator. The central axis of adjacent tooth tips is made offset by a distance $(K + 1/2)\tau$, and the electrical angle is $(L180° \pm 90°)$, where K and L are integers.

The operation principle of the FSPMLM can be described in Fig. 2.

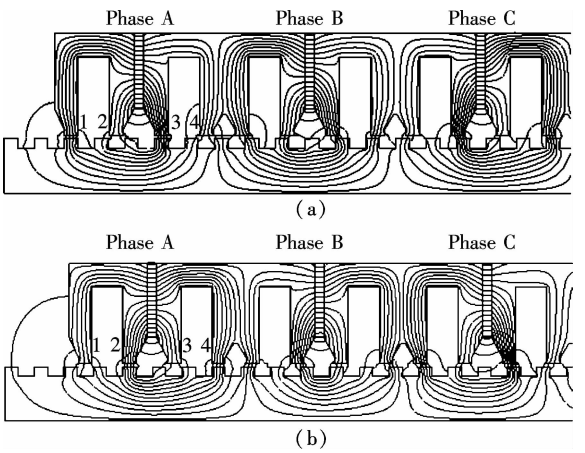

Fig. 2 The principle of the proposed FSPMLM. (a) Flux path of position 1; (b) Flux path of position 2

The open-circuit flux distributions of two typical positions are shown in Fig. 2. With the shift of the mover from position 1 to position 2, the main PM flux linked in this coil of phase A changes from negative maximum to positive maximum. The thrust force of the FSPMLM is generated under the co-effect of the changing flux and the armature current.

2 Electromagnetic Performance Analysis

The 2-D FEA model of the proposed FSPMLM is presented to investigate the static characteristics. The basic parameters of the three-phase FSPMLM used for simulation are listed in Tab. 1.

Tab. 1 Basic parameters of the FSPMLM

Items		Value/mm
Mover	Mover length	340
	Mover width	100
	Distance between phases	56.7
	Mover tooth width	4.5
	Space width between mover teeth	10.5
Stator	Stator tooth width	4.5
	Stator slot width	5.5
Air-gap	The length of air-gap	0.3

2.1 Flux-linkage and back-EMF

First, the open-circuit performance is analyzed by the FEA. When the value of the armature current is zero and the speed of the mover is 0.5 m/s, the waveforms of PM flux-linkage and open-circuit back EMF are obtained.

The PM flux linkage of phase B is shown in Fig. 3. Fig. 4 shows the three-phase open-circuit back-EMF waveforms of the FSPMLM.

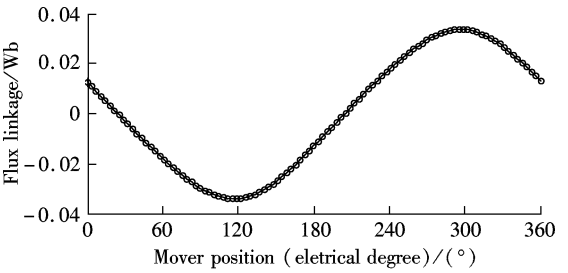

Fig. 3 The open-circuit PM flux linkage of phase B

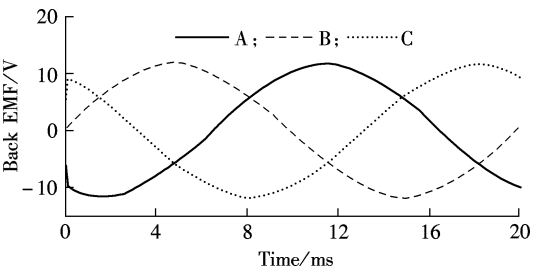

Fig. 4 Three-phase back-EMF waveforms

From Fig. 3, it can be seen that the waveform of the PM flux linkage is sinusoidal, and the value is not related to the speed of the mover but dependent on the position of the mover. From Fig. 4, one can see that the open-circuit back-EMF waveforms are sinusoidal. And the phase angle difference between the two phases is 120° of electrical degrees. Therefore, this FSPMLM can be driven as a brushless AC (BLAC) motor.

2.2 Inductance characteristic

To calculate the inductances of the FSPMLM, a DC current is injected into the armature winding. The flux linkage is determined by the total PMs and the armature current can be expressed as [9]

$$\psi = \psi_{pm} + Li \tag{1}$$

where ψ is the total flux linkage; ψ_{pm} is the open-circuit PM flux linkage; L is the inductance; i is the armature current.

It can be seen that the inductance of the FSPMLM is both determined by the physical position and the current of the armature coil. The characteristics of inductance are analyzed by the 2-D FEA. The inductions under different currents are obtained and compared.

The characteristics of self-inductances are shown in Fig. 5. From Fig. 5, it can be seen that the self-inductances have little change in value with the variation of position under a constant winding current. Therefore, the change of self-inductances can be ignored, when the value of the winding current is less than 10 A. However, when the current is over 10 A, the magnetic circuit is supersaturated. The self-inductance decreases with the increase in the winding current.

Fig. 6 shows the characteristics of mutual inductances. One can see that the mutual inductances change in value with the variation of position and the winding current. The values of mutual inductances are smaller than the values of self-inductances. Due to the cut-off of the primary iron

core, the mutual inductance between phase A and phase C is approximately zero.

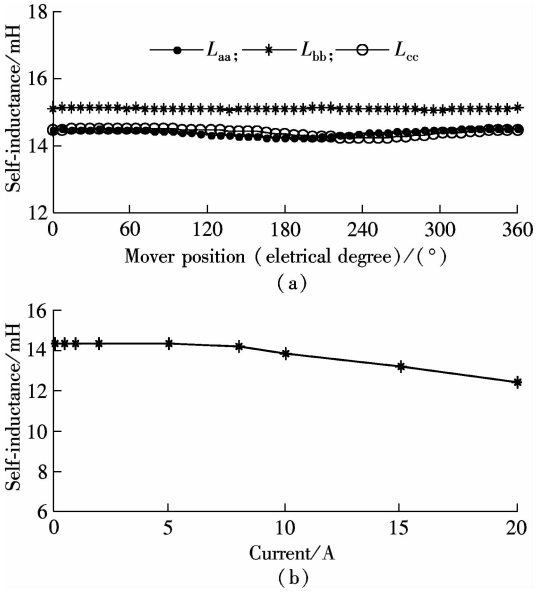

Fig. 5 Self-inductance characteristics of the FSPMLM. (a) Three phase self-inductance under 5 A winding current; (b) Self-inductance of phase A changing with winding current

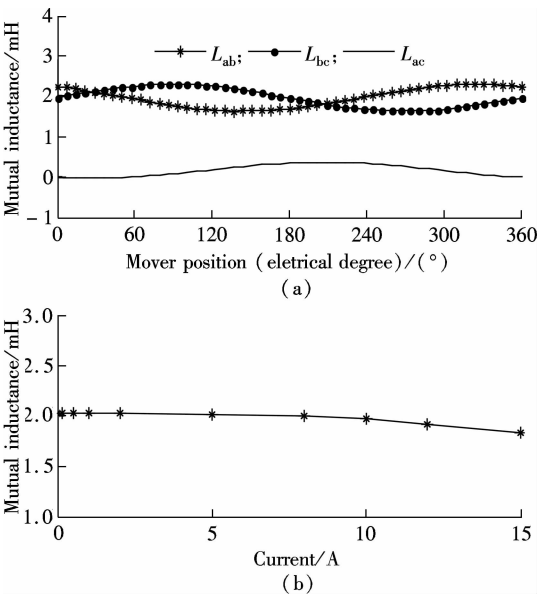

Fig. 6 Mutual inductance characteristics of the FSPMLM. (a) Mutual inductance under 5 A winding current; (b) Mutual inductance between the phase A and phase B changing with winding current

2.3 Cogging force characteristic

The cogging force is an unexpected parameter for the PM machine and it can cause the ripple of thrust and the mechanical vibrations, which may lead to undesirable damage. Hence, reducing the cogging force is the main purpose of the optimization of the PM machine.

The cogging force is produced by the interaction between the stator slot effect and the mover slot effect[10]. The structure of E-shaped stacks is helpful for reducing the cogging force. In order to investigate the influence of E-shaped stacks, another model of the FSPMLM with U-shaped stacks is built and shown in Fig. 7. There are twelve U-shaped stacks in the mover. Nonmagnetic displacers are positioned between the phases.

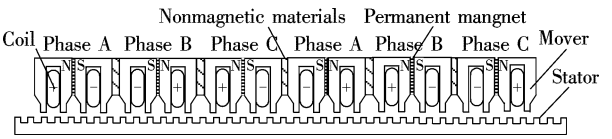

Fig. 7 2-D model of FSPM linear machine with U-shaped stacks

These two kinds of FSPMLMs are simulated by using the FEM. The cogging forces of two kinds of FSPMLMs are compared and shown in Fig. 8(a). The open-circuit back EMF of two kinds of FSPMLMs are shown in Fig. 8(b). FSPM1 is the FSPMLM with U-shaped stacks and FSPM2 is the one with E-shaped stacks.

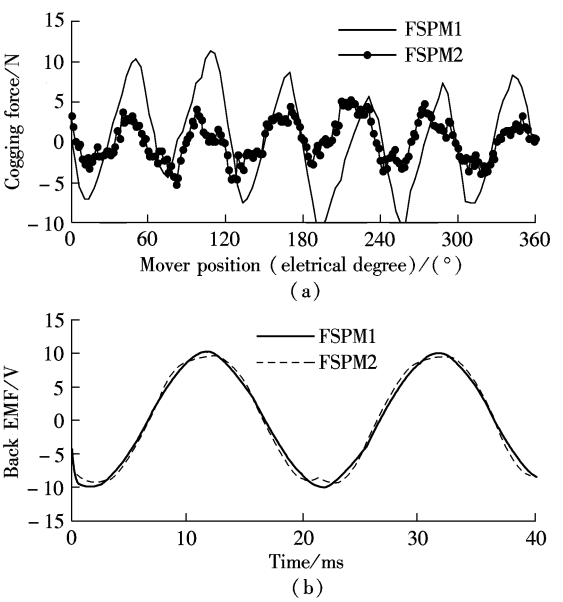

Fig. 8 Comparison of cogging force and back EMF between two kinds of FSPMLMs. (a) Cogging force of two FSPMLMs; (b) Open-circuit back EMF of two FSPMLMs

As shown in Fig. 8, the back EMF of the FSPMLM with E-shaped stacks is the same as that of the FSPMLM with U-shaped stacks. However, the cogging force of the one with E-shaped stacks is smaller than that of the other one. The results demonstrate that the cogging force is effectively reduced by using the E-shaped stacks and the thrust force will not be reduced.

2.4 Static thrust force

The co-energy method is employed to derive the thrust force equation. This process is similar to the one of the doubly-salient permanent magnet motor. According to the torque equation derived in Ref. [11], the thrust force of the FSPMLM can be expressed as

$$F_e = \frac{d}{dx}\left[\frac{1}{2}\boldsymbol{I}^T\boldsymbol{L}\boldsymbol{I} + \boldsymbol{\Psi}_m^T\boldsymbol{I}\right] + F_{cog} = F_r + F_{pm} + F_{cog} \quad (2)$$

$$F_r = \frac{1}{2}\boldsymbol{I}^T\left(\frac{d}{dx}\boldsymbol{L}\right)\boldsymbol{I} \quad (3)$$

$$F_{pm} = \frac{d}{dx}[\boldsymbol{\Psi}_m^T\boldsymbol{I}] \quad (4)$$

where $\boldsymbol{I} = [i_a, i_b, i_c]^T$; $\boldsymbol{\Psi}_m = [\psi_a, \psi_b, \psi_c]^T$; $\boldsymbol{L} = [L_{ij}]^T (i = a, b, c;\ j = a, b, c)$; x is the direction of motion; F_{cog} is the cogging force generated by slot effect.

The change of inductance is so little that it can be ignored before the magnetic circuit is supersaturated. If the harmonic of the flux-linkage is ignored and the end effect is not considered, the reluctance thrust component F_r can be ignored and the thrust equation changes into

$$F_e \approx \frac{d}{dx}(\boldsymbol{\Psi}_m)^T \boldsymbol{I} + F_{cog} = F_{pm} + F_{cog} \tag{5}$$

Assuming that the zero phase point of phase A flux-linkage is the position zero of the mover, the PM thrust component F_{pm} can be expressed as

$$F_{pm} = \frac{d\psi_a}{dx} i_a + \frac{d\psi_b}{dx} i_b + \frac{d\psi_c}{dx} i_c = 3\left(\pi \frac{1}{\tau}\right)\psi_m I_m \sin\alpha \tag{6}$$

where ψ_m is the amplitude of the fundamental PM flux-linkage component; I_m is the amplitude of armature current; and α is the phase separation between the open-circuit PM flux-linkage and the armature current.

At operation, the phase angle of the current is in sync with the phase angle of the no-load back EMF when $\alpha = 90°$. From Eq. (6), it can be seen that the thrust is only determined by the virtual value of the phase current under an invariable air-gap. The speed is only determined by the frequency of the phase current.

The 2-D transient FEM is employed to analyze the transient thrust force of the FSPMLM. The simulation result of the thrust force under 3 A current load is shown in Fig. 9, and the thrusts of simulation and calculation with different loads are shown in Fig. 10.

As shown in Fig. 9, the value of thrust calculated by Eq. (6) is 140 N, and the average value of simulated thrust obtained by the FEA is 138 N. There is a good agreement between them.

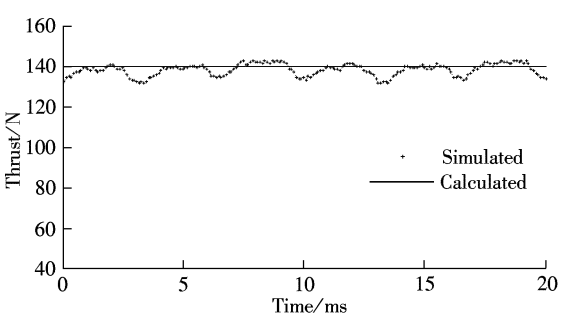

Fig. 9 The thrust force of 3A in the windings

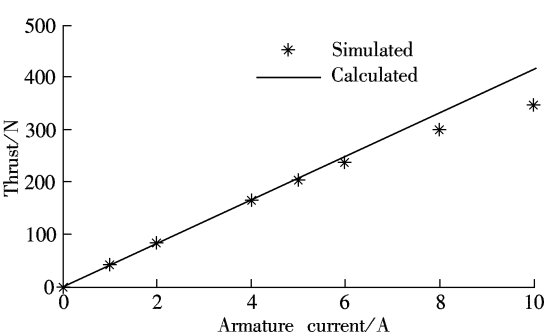

Fig. 10 Thrust with different currents

From Fig. 9 and Fig. 10, one can see that the results of the simulation verify the correctness of the thrust equation. When the virtual value of the winding current is above 8 A, the results of the simulation are less than the calculated results because of the increase of magnetic circuit saturation.

3 Experimental Validation

An experimental mode is used to test the operation performance and verify the results of FEA and calculation. The data of the prototype is the same as that of the simulation model listed in Tab. 1. The measured open-circuit back EMF is shown in Fig. 11(a), and the measured current of one phase at 140 N loading resistance is shown in Fig. 11(b).

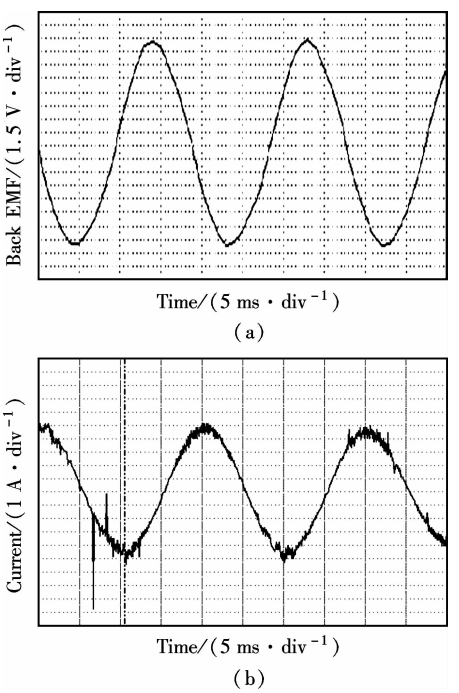

Fig. 11 Experimental results. (a) Open-circuit back EMF at speed of 0.5 m/s; (b) Measured current at 140 N resistance

Comparing the results of simulation and experimentation, it can be seen that a good agreement is achieved between simulated and measured results. All the results validate the correctness of the analyzed static characteristics of the proposed FSPMLM.

4 Conclusion

A novel flux-switching permanent magnet linear machine is proposed for linear direct driving machine tools. The electromagnetic performance is investigated by using the 2-D FEM. The thrust equation is derived and verified by the simulation results. Finally, a prototype is used to certify the analysis results of electromagnetic performance. The experimental results agree with the simulation results. All the results demonstrate that this kind of FSPMLM has advantages of simple secondary structure, high thrust force density, minimal cogging force and low costs. This kind of linear motor has prospective application in long distance linear motion.

References

[1] Nasar S A, Boldea I. *Linear motor electric machines* [M]. New York: Wiley, 1976: 1 - 30.

[2] Isfahani A H, Ebrahimi B M, Lesani H. Design optimization of a low-speed single-sided linear induction motor for improved efficiency and power factor [J]. *IEEE Transactions on Magnetics*, 2008, **44**(2): 266 - 272.

[3] Stumberger G, Zarko D, Aydemir M, et al. Design and comparison of linear synchronous motor and linear induction motor for electromagnetic aircraft launch system [C]//*IEEE International Electric Machines and Drives Conferences*. Madison, WI, USA, 2003: 494 - 500.

[4] Rauch S E, Johnson L J. Design principle of flux-switching alternator [J]. *AIEE Transactions*, 1955, **74**(3): 1261 - 1268.

[5] Wang C F, Shen J X, Wang L L, et al. A novel permanent magnet flux-switching linear motor [C]//*The Fourth IET Conference on Power Electronics, Machines and Drives*. York, UK, 2008: 116 - 119.

[6] Zhu Z Q, Chen X, Chen J T, et al. Novel linear flux switching permanent magnet machines [C]//*International Conference on Electrical Machines and Systems*. Wuhan, China, 2008: 2948 - 2953.

[7] Wang Canfei, Shen Jianxin, Wang Yu, et al. A new method for reduction of detent force in permanent magnet flux-switching linear motors [J]. *IEEE Transactions on Magnetics*, 2009, **45**(6): 2843 - 2846.

[8] Jin Mengjia, Wang Canfei, Shen Jianxin, et al. A modular permanent magnet flux-switching linear machine with fault tolerant capability [J]. *IEEE Transactions on Magnetics*, 2009, **45**(8): 3179 - 3186.

[9] Hua Wei, Cheng Ming. Inductance characteristics of 3-phase flux-switching permanent magnetic machine with doubly-salient structure [J]. *Transactions of China Electrotechnical Society*, 2007, **22**(11): 21 - 28.

[10] Zhu Z Q, Thomas A S, Chen J T, et al. Cogging torque in flux-switching performance magnet machines [J]. *IEEE Transactions on Magnetics*, 2009, **45**(10): 4708 - 4711.

[11] Chau K T, Cheng Ming, Chan C C. Performance analysis of 8/6-pole doubly salient permanent magnet motor [J]. *Electric Power Components and Systems*, 1999, **27**(10): 1055 - 1067.

新型磁通切换永磁直线电动机的静态特性

黄 磊 余海涛 胡敏强 周士贵 刘合祥

(东南大学电气工程学院,南京 210096)

(东南大学伺服控制技术教育部工程研究中心,南京 210096)

摘要:提出了一种应用于直线驱动数控机床的新型磁通切换永磁直线电动机. 首先,给出了该电机的二维和三维拓扑结构,介绍了该直线电动机的基本工作原理,并分析了 2 种典型位置的磁场情况. 其次,采用二维有限元的方法,对电机的磁链特性、反电动势特性、电感特性等静态特性进行了深入的研究. 对 2 种不同铁芯结构磁通切换永磁直线电机的定位力进行了对比分析,结果表明采用 E 型铁芯机构可有效减少定位力. 然后,基于联合能量法推导得到了电机的静态推力计算公式,采用有限元仿真对静态推力计算公式进行了验证分析. 最后,通过一台试验样机进行了空载反电动势和负载试验测试. 仿真和实验结果表明该电机具有正弦度很好的反电动势、很小的定位力和高的推力密度, 适合应用于直线驱动的数控机床.

关键词:磁通切换;直线永磁电机;有限元方法;静态特性

中图分类号:TM359